

RotoWrist: Continuous Infrared Wrist Angle Tracking using a Wristband

Farshid Salemi Parizi
farshid@cs.washington.edu
Facebook Reality Labs, University of
Washington, United States

Wolf Kienzle
wkienzle@fb.com
Facebook Reality Labs, United States

Eric Whitmire
ewhitmire@fb.com
Facebook Reality Labs, United States

Aakar Gupta
aakarg@fb.com
Facebook Reality Labs, United States

Hrvoje Benko
benko@fb.com
Facebook Reality Labs, United States



Figure 1: RotoWrist is a wristband that can track 2-DoF continuous relative angle of the wrist with respect to the arm. Left: A user playing Beat Saber with an Oculus Rift-S VR system. The left hand orientation is estimated using RotoWrist while a Rift-S controller tracks the right hand. Middle: Visualization of wrist angle tracking in a Unity test application. Right: RotoWrist tracking relies on eight time of flight IR modules embedded in a wristband.

ABSTRACT

We introduce RotoWrist, an infrared (IR) light based solution for continuously and reliably tracking 2-degree-of-freedom (DoF) relative angle of the wrist with respect to the forearm using a wristband. The tracking system consists of eight time-of-flight (ToF) IR light modules distributed around a wristband. We developed a computationally simple tracking approach to reconstruct the orientation of the wrist without any runtime training, ensuring user independence. An evaluation study demonstrated that RotoWrist achieves a cross-user median tracking error of 5.9° in flexion/extension and 6.8° in radial and ulnar deviation with no calibration required as measured with optical ground truth. We further demonstrate the performance of RotoWrist for a pointing task and compare it against ground truth tracking.

CCS CONCEPTS

• **Human-centered computing** → Ubiquitous and mobile computing; Pointing devices; Pointing.

KEYWORDS

wrist pose; time-of-flight sensor; virtual and augmented reality; hand tracking; wearable device; wristband.

ACM Reference Format:

Farshid Salemi Parizi, Wolf Kienzle, Eric Whitmire, Aakar Gupta, and Hrvoje Benko. 2021. RotoWrist: Continuous Infrared Wrist Angle Tracking using a Wristband. In *27th ACM Symposium on Virtual Reality Software and Technology (VRST '21)*, December 8–10, 2021, Osaka, Japan. ACM, New York, NY, USA, 11 pages. <https://doi.org/10.1145/3489849.3489886>

1 INTRODUCTION

Wearable devices have grown immensely popular and are enabling computing in many areas of people’s lives across a wide range of scenarios. Tracking the movement of the hand has long been important in developing natural and intuitive interaction paradigms for computing [32]. Specifically, the dexterity of human wrist joints typically enables a broad range of motion [23], making the wrist a promising modality to drive input for wearable computing.

Existing hand tracking methods most often rely on computer vision [5, 24, 27, 29, 35, 39] with cameras in the environment or on a head-mounted display (HMD). These approaches yield high accuracy, but require line-of-sight and in some cases, infrastructure

Permission to make digital or hard copies of all or part of this work for personal or classroom use is granted without fee provided that copies are not made or distributed for profit or commercial advantage and that copies bear this notice and the full citation on the first page. Copyrights for components of this work owned by others than the author(s) must be honored. Abstracting with credit is permitted. To copy otherwise, or republish, to post on servers or to redistribute to lists, requires prior specific permission and/or a fee. Request permissions from permissions@acm.org.

VRST '21, December 8–10, 2021, Osaka, Japan

© 2021 Copyright held by the owner/author(s). Publication rights licensed to ACM.

ACM ISBN 978-1-4503-9092-7/21/12...\$15.00

<https://doi.org/10.1145/3489849.3489886>

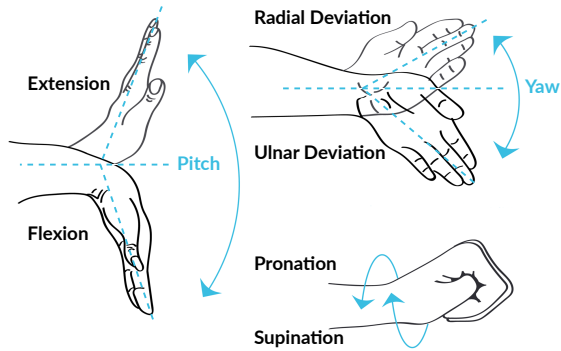


Figure 2: Diagram illustrating different wrist motions. RotoWrist continuously captures wrist flexion/extension and radial/ulnar deviation. It does not attempt to capture pronation/supination.

support, that limit mobility and versatility. The growing demand for computing in ubiquitous contexts motivates researchers to consider wrist-worn devices (e.g., smartwatches and smart bands), which have become increasingly mainstream. However, most research efforts around wristband-based sensing focus on discrete, gesture based interactions [6, 8, 9, 13, 14, 36, 43, 45]. Although discrete gestures are useful, they are just one part of the interaction language needed for mobile wearable computing. For common tasks like pointing at targets, drawing, sliding, or swipe-based text input, an input device that supports continuous tracking will be most appropriate.

In this work, we present RotoWrist, an infrared (IR) light-based device that performs continuous 2-degree-of-freedom (DoF) wrist tracking from the wristband. RotoWrist works without requiring any user training. The RotoWrist system consists of a wristband that uses eight ToF IR modules to continuously estimate the 2-DoF angle of the wrist with respect to the forearm in real-time. Each low-power sensor measures the absolute distance from the hand. As the user moves their wrist, the relative distance between the hand and each sensor changes. RotoWrist combines these eight measurements into a 2-DoF wrist orientation—flexion/extension and radial/ulnar deviation, as depicted in Figure 2.

Among related work in sensor-based tracking of the wrist, RotoWrist is most similar to WristWhirl[9]. In RotoWrist, we prioritized robustness and accuracy and designed the system from ground up to support continuous, absolute tracking without any user calibration. While the WristWhirl system is capable of sensing continuous wrist motion, it did not investigate tracking performance and focused primarily on the accuracy of detecting 8 distinct gestures. Not only does RotoWrist support real-time continuous tracking that is benchmarked against a ground truth system, but we further establish RotoWrist’s ability to operate in a cross-session and cross-user fashion.

RotoWrist offers a rich input source for a variety of wearable devices, including smartwatches and HMDs. With RotoWrist, a user

can provide continuous input using their wrist, in eyes-away contexts where line-of-sight to a camera might be difficult to maintain. For example, user might point while keeping their arm motionless at their side or with their hands beneath a table.

Our primary contributions are:

- (1) A simple, low-power hardware architecture consisting of eight time-of-flight IR light modules embedded in a custom-built wristband that enables continuous wrist angle tracking.
- (2) A tracking algorithm that can reliably estimate 2-DoF orientation of the wrist without user training.
- (3) A system characterization and user evaluation demonstrating tracking accuracy of 5.9° in flexion/extension and 6.8° in radial/ulnar deviation across users without any calibration, compared to an optical motion capture system.
- (4) A study comparing RotoWrist’s pointing performance to a high-precision wrist and forearm tracker.

2 RELATED WORK

Existing hand tracking methods are based on sensors that are either outside-in (off-body) or inside-out (on-body). Outside-in sensors with cameras [5, 24, 27, 29, 35, 39] or radio frequency[21, 38] employ external sensing infrastructure that limits users’ mobility for daily interaction and making these technologies less suited to mobile and ubiquitous uses. In comparison, inside-out sensing approaches provide much better mobility support. Therefore, in the rest of this section we have focused on inside-out hand tracking and have split the related work into two main categories: 1) tracking wrist movement by leveraging the internal anatomy of the wrist and 2) tracking using the external contours of the hand.

2.1 Inferring wrist angles from internal signals

A number of research projects explored electromyography (EMG) where electrodes are placed below the elbow to detect hand gestures [16, 31]. EMG systems are complex and require the user to wear a bulky array of electrodes below the elbow. Although these systems continuously track user wrist and fingers, they require a very exhaustive training and/or calibration. Other researchers have leveraged electrical impedance tomography [45], bio-capacitive sensing [28, 36], IR tomography [22], acoustic tomography [7, 11] and more recently ultrasound [14] for discrete hand gesture recognition from a wristband. These methods result in discrete, gesture-based interactions like detecting a fist vs stretch, directional sweep, finger pinches, and not continuous tracking. Furthermore, these systems are often very sensitive to the positioning and slippage of the device and therefore often require per-session training.

2.2 Inferring wrist angles from external signals

Skin surface deformation due to wrist movement can be detected by pressure/stretch sensors [6, 15, 34]. Other researchers have leveraged ultrasound beam forming [13] and acoustics [19, 25] to recognize discrete gestures. Other approaches to determining hand pose on wearable devices employ vision sensors such as a camera or optical sensor on the inner side of the arm or wrist [9, 18, 41, 44]. Digits [18] used infrared illumination from the wrist to track hand pose. Opisthenar uses an embedded wrist camera to recognize static

hand poses [44]. Although this method can enable full hand tracking, the form factor and power consumption limits practicality. FingerTrak use 4 thermal cameras around the wrist to reconstruct full hand pose though cannot reconstruct relative angle of the wrist with respect to the forearm and consumes around 3 watts of power which limits practicality in a mobile setting [12].

WristWhirl [9] is most relevant to RotoWrist. It uses an array of proximity sensors that can detect gestures with high quality. Our work advances upon WristWhirl in four significant aspects: 1) RotoWrist investigates and reports real-time angular deviations from the ground truth. WristWhirl did not investigate tracking performance, focusing primarily on the accuracy of detecting 8 distinct gestures including 4 directional marks, and 4 free-form shapes. 2) For angular wrist pose estimation, we establish RotoWrist’s cross-session and cross-user performance. In contrast, WristWhirl only reported within-session performance and required the user to calibrate every session. 3) In addition to raw sensing accuracy, we further investigate RotoWrist on a pointing task and compare its performance with ground truth. It’s unclear how well WristWhirl can be used for pointing tasks. 4) RotoWrist improves upon WristWhirl’s hardware design by adopting optical ToF sensors which are robust to different skin tones, lighting conditions, and indoor vs. outdoor use. WristWhirl’s IR photo diode based approach is prone to ambient IR noise, lighting changes, and skin tone dependencies owing to variations in IR light reflection from the skin.

There is also a line of work on using a ring in tandem with a wristband for finger tracking and gesture interaction. Magic Finger [42] and Light Ring [17] enables users to interact with surfaces using optical sensor embedded in a wearable ring form factor. WRIST [43] explores combining IMU data from a smartwatch and smart ring for distal pointing and gesture interaction. Researchers have also used magnetic tracking for wrist and finger tracking [3, 4, 26].

In addition, many commercial augmented and virtual reality systems primarily use a handheld controller to continuously track users’ hand pose. While these solutions offer great accuracy and specific affordances, they are still limited by mobility constraints. Tracking the hand without controllers and without line-of-sight affords the potential to consider new freehand interactions. RotoWrist is the first wrist-mounted device that can reconstruct wrist angle continuously by using eight ToF IR modules sitting tightly on the wrist. A key innovation of RotoWrist is that it does not require users any training before using the system thus making it work out of the box.

3 IMPLEMENTATION

The RotoWrist system consists of a sensing wristband that incorporates eight ToF IR modules and a controller arm band that handles powering the sensing wristband and communicating the data back to a host PC. The following sections provide details of the RotoWrist hardware, capabilities and algorithm.

3.1 Sensing Wristband

One of the challenging aspects of designing a wristband is to manufacture one that can fit different people and whose sensing is robust to different wrist sizes. In addition, the form-factor of the wristband should be minimally invasive. We design the wristband as a top

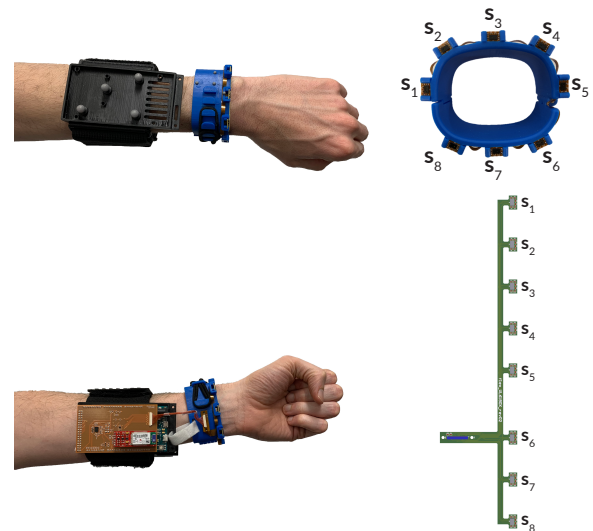


Figure 3: RotoWrist consists of a controller arm band that handles communicating the data back to host PC and eight time-of-flight modules embedded in a wristband.

and bottom part that connect together using a hinge mechanism. All parts are made using a 3D printed Nylon material. The hinge (Figure 1 right) on the side allows the band to open and close. On the other side, we have leveraged an elastic band to securely fasten the top and bottom parts. As shown in Figure 3 left, there are several hooks on the top part that the elastic band can be connected to based on the wrist size. To further support people with different wrist sizes, we built two sizes of the sensing wristband – one with a diameter of 120 mm and the other 180 mm.

As shown in Figure 3 (bottom right), we built a custom flex PCB that incorporates eight time of flight modules (VL6180X) and a 22-pin SMD connector. These modules are equally spaced around the wristband and they sit perpendicular to and at most 8 mm from the wristband’s surface. Each individual sensor determines the distance to the nearest object within a 25° cone by emitting pulsed infrared light and timing the returned reflection. The eight TOF modules consume only 13.6 mA.

3.2 Controller Armband

The sensors on the wristband are connected to a custom made daughterboard through a very thin 22 pin assembly cable¹. Since the recommended operating voltage for the ST ToF module is 2.8 V, the daughterboard also incorporates two bidirectional level-shifting translators (TXB0106). As shown in Figure 3 (bottom left), the daughter board sits on an Arduino Due. The sensors on the wristband are connected to the microcontroller (Atmel SAM3X8E ARM Cortex) on the Due board over I²C, which triggers measurement. A timer-based algorithm is set to take measurement every 20 ms from all the sensors resulting in a tracking frame rate of 50 Hz. A SparkFun Bluetooth Mate Silver module also sits on top of the daughter

¹ A22XSR22XSR36R254B

board to facilitate sending the data to a host PC over Bluetooth. Using Velcro tape, the armband also hold a small battery pack that powers the Arduino and other components on the board.

3.3 Tracking Algorithm

We use a ToF-sensing array to track wrist orientation by comparing the distance measurement from each sensor to the hand. The conical fields of view of each individual ToF sensor overlap significantly, so several sensors simultaneously produce an in-range sensor measurement. As parts of the hand move in and out of the field of view of each ToF sensor, the distance reading from that sensor becomes smaller and larger.

We use a simple tracking algorithm that reliably tracks wrist orientations across different users. As shown in Figure 3, we name each sensor in a clockwise fashion starting on the radial side from S_1 to S_8 . As expected, we observe that the topmost (S_2, S_3, S_4) and bottommost (S_6, S_7, S_8) sensors have the most linear effect when there is a flexion/extension activity (i.e. pitch) and the sensors on the radial (S_8, S_1, S_2) and ulnar (S_4, S_5, S_6) sides are most responsive to radial/ulnar deviation (i.e. yaw). We model these observations using Equations 1 and 2 where D_{S_i} refers to the distance value that is returned by the sensor S_i at a certain point in time. For each of the equations, there is a weight term associated with each of the sensors ($W_{S_i}^p$ and $W_{S_i}^y$) which defines the individual weight given to a particular sensor and (B_p and B_y) refer to a bias offset value.

$$Pitch = \left(\sum_{i=2,3,4} \frac{W_{S_i}^p}{D_{S_i}} - \sum_{i=6,7,8} \frac{W_{S_i}^p}{D_{S_i}} \right) + B_p \quad (1)$$

$$Yaw = \left(\sum_{i=1,2,8} \frac{W_{S_i}^y}{D_{S_i}} - \sum_{i=4,5,6} \frac{W_{S_i}^y}{D_{S_i}} \right) + B_y \quad (2)$$

These 14 parameters (7 each in pitch and yaw) are learned in a user evaluation explained in Section 5. We formulated the problem as a non-linear optimization problem which we solved using a Levenberg-Marquardt algorithm.

4 USER EVALUATION SETUP

A ground truth system is required to evaluate RotoWrist orientation accuracy. Since the wrist is not a rigid body and the skin is stretchable, tracking the angle of the wrist with respect to the arm is challenging. The most precise method of measuring the wrist angle is to use radiographs to measure the carpal bone angle on lateral wrist [20]. Prior research has looked at building a custom-made calibration device that has pivot joints with potentiometers to measure the wrist angle [37]. Since building such devices would affect the IR reading from our wristband (due to the calibration device occluding the IR sensors) and doing radiographs is not practical, we used a fifteen-camera OptiTrack² motion capture system to record the real-time pose of the wrist, forearm, and hand stub at 240 Hz. We placed retro-reflective spheres on both the controller armband and sensing wristband in known locations, as shown in Figure 4. The participant wore the wristband and armband on their left hand

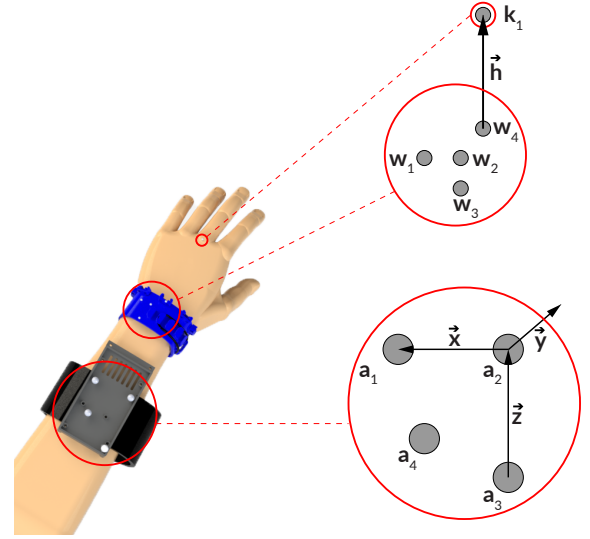


Figure 4: Retro-reflective markers placed on the wristband, armband and middle finger knuckle to facilitate tracking.

and a researcher placed a small IR retro-reflective marker on their middle finger metacarpophalangeal joint.

We placed the armband retro-reflective markers in a way that two of the four are in the direction of the arm (markers a_2 and a_3), and two are perpendicular to the arm (markers a_1 and a_2) as shown in Figure 4. The markers (a_1, a_2, a_3) define our arm coordinate frame:

$$\vec{z} = a_2 - a_3 \quad \vec{x} = a_1 - a_2 \quad \vec{y} = \vec{z} \times \vec{x} \quad (3)$$

We also placed four retro-reflective markers on the sensing wristband. Markers $w_1, w_2,$ and w_3 are used to help track the arm orientation in Section 6. w_4 is placed on the top middle part of the wristband and, together with k_1 , defines the wrist orientation vector as $\vec{h} = k_1 - w_4$. The placement of w_4 and k_1 markers is chosen so that when a person has a neutral hand pose (i.e. zero pitch and yaw), \vec{h} is parallel to \vec{z} and perpendicular to \vec{x} . Given the wrist orientation vector \vec{h} and the arm coordinates ($\vec{x}, \vec{y}, \vec{z}$), pitch and yaw of the wrist can be defined as follow:

$$pitch = \arccos(\vec{h} \cdot \vec{y}) \quad yaw = \arccos(\vec{h} \cdot \vec{x}) \quad (4)$$

5 USER EVALUATION 1: ANGULAR ACCURACY

We performed two focused studies to evaluate the performance of RotoWrist. The first study evaluates the dynamic tracking accuracy of our system compared to a motion capture ground truth system. Maintaining performance across worn sessions (i.e., reworn at a later time) or between different people is a challenge for almost all bio-sensing and wearable systems, since misalignment could result in signal change. The following sections evaluates the robustness of RotoWrist in different scenarios.

²OptiTrack Prime 17W

We recruited 14 people (25-59 years old, Mean: 32) to evaluate the tracking accuracy of our system. The study took less than 30 minutes and participants were compensated for their time. Upon arrival, we asked the participants to sit on a chair while putting their left arm on a table that was in front of them. A researcher helped the participants put on the wrist and arm band and the retro-reflective marker on the left hand of the user as explained in Section 4. Based on their wrist sizes, five people wore the smaller sized wristband and the other nine were given the larger wristband. The wristband was placed where a user might typically wear a smartwatch (roughly at the tip of the ulna) as depicted in Figure 3. Using the elastic bands, the wristband was fit to the user making sure they can move their wrist without discomfort. The location of the armband is roughly placed in the middle of the forearm in a way that the markers are facing the user. For consistency, we asked users to maintain a fist pose throughout the study. Anecdotally, RotoWrist is robust to different finger poses, though we have not fully evaluated this effect.

The evaluation was conducted in two sessions and each session had two phases. *Phase 1, Defined motion*: Participants were asked to hold their wrist in a neutral position in the beginning of each session and then perform three flexion/extension and three radial/ulnar deviation movements, exercising their full, comfortable range of motion. *Phase 2, Random motion*: Participants performed 4 minutes of free-form movements while being asked to exercise all possible wrist joints motions. After the two phases in the first session, the wristband was taken completely off. The users were instructed to take a minimum of 2 minutes of break. After the break, the researcher asked the participants to put the wristband back on, and the same procedure was given to the user and the two phases were repeated.

Once data has been recorded from both the 50 Hz RotoWrist system and the 240 Hz motion capture system, we must align and synchronize the two data streams. Such a synchronization requires the comparison of correlated events in each data stream, but the raw sensor data is uncorrelated with the ground truth wrist orientation given by Equations 4. To address this challenge, we use the time-alignment technique presented in [40]. We compare the ground truth wrist orientation with an approximation of pitch and yaw specified by Equation 5 and 6. We use these signals to achieve alignment at the start and end of the recorded data streams. We then resample the motion capture system through interpolation to 50 Hz to achieve frame-by-frame alignment with the RotoWrist.

$$Pitch_{apx} = 150 \times \left(\sum_{i=2,3,4} \frac{1}{D_{S_i}} - \sum_{i=6,7,8} \frac{1}{D_{S_i}} \right) \quad (5)$$

$$Yaw_{apx} = 200 \times \left(\sum_{i=1,2,8} \frac{1}{D_{S_i}} - \sum_{i=4,5,6} \frac{1}{D_{S_i}} \right) \quad (6)$$

After synchronization, we formulated the problem as a non-linear optimization problem which we solved using a Levenberg-Marquardt algorithm. The cost function for this optimization problem was set to be the difference in the pitch and yaw estimation from Equation 1 and 2 and the angles calculated from motion capture system using Equation 4 (Section 4).

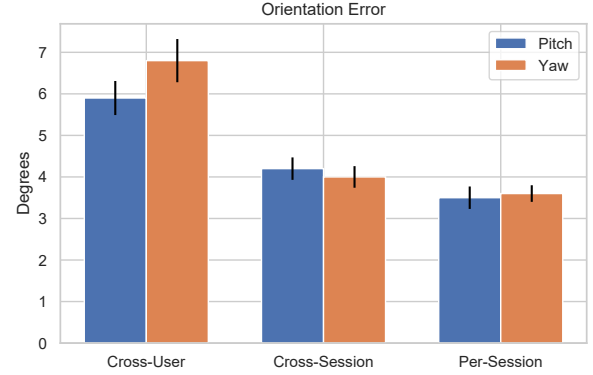


Figure 5: Shows the root mean square error and standard deviation among 14 participants using the three models.

Although using a motion capture system to capture the ground truth of the orientation of the wrist with respect to the forearm is practical, this method does not capture the full complexity of the human hand anatomy. For example, in a neutral pose (i.e both pitch and yaw are zero), we expect that the \vec{h} is perfectly aligned with \vec{z} . This is not always true due to the geometry of the hand. Therefore in evaluating RotoWrist, we add a one time offset, to force the pitch and yaw estimation from Equations 1 and 2 to start at zero. This offset is only required to compare RotoWrist estimates with the wrist orientation derived from ground truth and is not necessary for normal operation. We evaluate the tracking accuracy of RotoWrist in three different categories: 1) cross-user where no calibration is needed, 2) cross-session, and 3) per-session where a user can perform a short calibration.

5.1 Cross-User Evaluation

As stated in Section 1, a widespread input solution should be robust and extensible (e.g. supporting different users and contexts out of the box). Therefore, in this section, we evaluate how our tracking holds between users. Notably, we learned the heuristic model parameters presented in Section 3.3 on only phase 1 (defined motion) from the first session of all participants except one and tested on all of the data (including phases 1 and 2) from the left out user. We repeat this for all of the participants. We learn a total of 14 parameters for this evaluation: 12 individual sensor weights, and 2 bias terms. The measured root mean square error (RMSE) for pitch and yaw across users is 5.9° and 6.8° respectively.

5.2 Cross-Session Evaluation

To quantify how the performance holds when worn by the same user, we ran a leave-one-session-out cross validation for each of our participants. We learned the same heuristic model parameters presented in Section 3.3 on only phase 1 (defined motion) from session one. After learning these parameters, we test on all data (phases 1 and 2) from session two. The pitch and yaw RMSE in degrees across all users is 4.2° and 4.0° respectively.

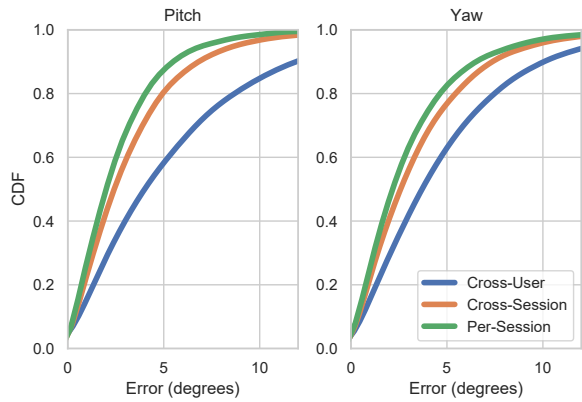


Figure 6: Cumulative distribution function of pitch and yaw orientation tracking error.

5.3 Per-Session Evaluation

Although we don't expect users to calibrate RotoWrist each session, to better shine a light on how the tracking improves with a very small calibration procedure, we evaluate RotoWrist's per-session accuracy. To do this, we learned the heuristic model parameters (Equations 1 and 2) from phase 1 of each session and tested on phase 2 of the same session. The pitch and yaw RMSE in degrees using this calibration reduces to 3.5° and 3.6° respectively. We summarized these results in Figure 5.

Figure 6 shows the cumulative distribution function (CDF) of orientation accuracy between all three evaluations discussed above. Figure 7 shows the spatial distribution of orientation tracking error of the cross-user model projected onto a 2D plane among all users. As depicted and expected, due to kinematics of the wrist, users performed more negative yaw (flexion) and negative pitch (radial deviation) movement which is aligned with the functional ranges of the wrist joint motions [30]. Due to the geometry of the wrist, the trapezoid bone and the thumb are placed slightly outside of the forearm axis and because of that the performance of RotoWrist is relatively better in radial than ulnar deviation as shown in Figure 7.

6 USER EVALUATION 2: POINTING

We conducted a second study to evaluate RotoWrist on a pointing task. Through this study we aim to understand whether RotoWrist's accuracy is sufficient for a pointing task and how this performance compares with respect to ground truth wrist tracking and ground truth forearm tracking. Forearm tracking can also be enabled via wrist-worn sensing [2, 33], but involves large, fatiguing arm movements, and thus is a contrasting point of comparison to wrist tracking. We further evaluate how well RotoWrist pointing adheres to Fitts' law.

6.1 Design

Since the yaw motion range is smaller than the pitch, more research is needed into how the angular movement across different wrist rotational axes is mapped to the on-screen cursor. Prior work [10]

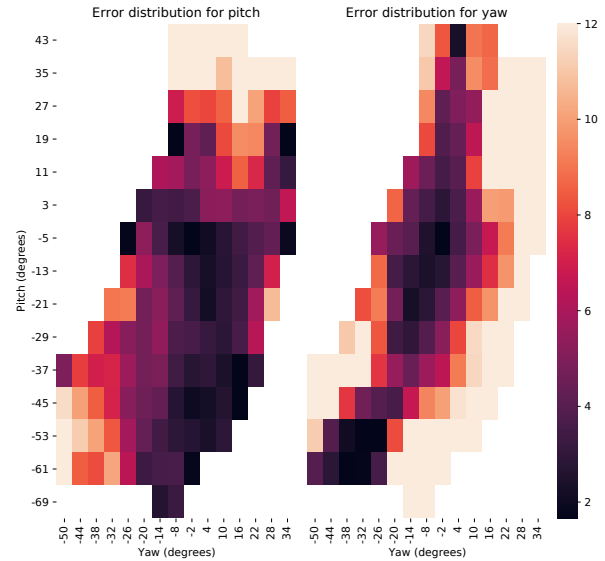


Figure 7: Heatmap showing spatial distribution of error among all users for cross-user evaluation.

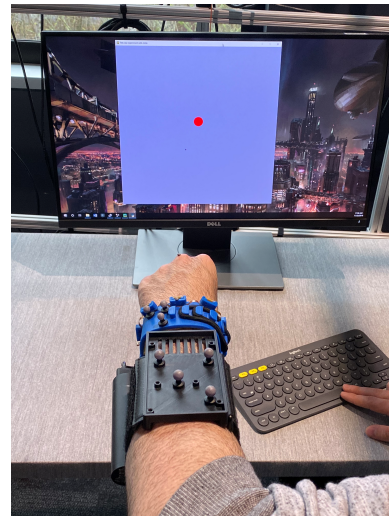


Figure 8: 2D pointing study setup. Users sit on a chair and use the space bar of a keyboard for target selection.

has shown that a mismatched mapping function between the different wrist motion axes can still yield useful results. To keep things simple, we conducted the pointing evaluation along the yaw and pitch axes separately and in our 2D pointing study, we mapped the yaw and pitch movements to a relative cursor movement (in the x and y direction) on a nearby large display. For each of the two axes (yaw and pitch), we had three independent variables: *Method* (GTF - Ground Truth Forearm Tracking, GTW - Ground truth Wrist Tracking, R - RotoWrist), *Distance* (Pitch: 100, 200, 400 pixels; Yaw: 50, 100, 200 pixels), *Width* (20, 40, 60 pixels) resulting in $2 \times 3 \times 3 \times 3 = 54$ conditions. The distance and width conditions

Table 1: Pointing Study: 3-way ANOVA Main effects and pairwise comparisons. No interaction effects were found.

	Condition	ANOVA	Pairwise Comparisons
Yaw MT	Method	$F(2, 22) = 9.252, p < 0.005, \eta^2 = .457$	$GTW < GTF(p < .05), GTW < R(p < .05)$
	Distance	$F(2, 22) = 40.897, p < 0.001, \eta^2 = .788$	$50 < 100 < 200 (p < .05)$ for all
	Width	$F(2, 22) = 48.817, p < 0.001, \eta^2 = .816$	$60 < 20(p < .001), 40 < 20(p < .001)$
Yaw IT	Method	$F(2, 22) = 7.558, p < 0.005, \eta^2 = .407$	$GTW < GTF(p < 0.005)$
	Distance	$F(2, 22) = 7.064, p < 0.005, \eta^2 = .391$	$50 < 200(p < .05), 100 < 200(p < .05)$
	Width	$F(1.29, 14.19) = 8.54, p < 0.01, \eta^2 = .437$	$60 < 20(p < .05), 40 < 20(p < .05)$
Pitch MT	Method	$F(2, 22) = 13.034, p < 0.001, \eta^2 = .542$	$GTW < GTF(p < .005), GTW < R(p < .05)$
	Distance	$F(2, 22) = 34.115, p < 0.001, \eta^2 = .756$	$100 < 200 < 400(p < .05)$ for all
	Width	$F(2, 22) = 36.413, p < 0.001, \eta^2 = .768$	$60 < 40 < 20(p < .05)$ for all
Pitch IT	Method	$F(2, 22) = 6.862, p < 0.01, \eta^2 = .384$	$GTW < GTF(p < .05), GTW < R(p < .05)$
	Distance	$F(2, 22) = 11.004, p < 0.001, \eta^2 = .500$	$100 < 400(p < .05), 200 < 400(p < .05)$
	Width	$F(2, 22) = 19.947, p < 0.001, \eta^2 = .645$	$60 < 20(p < .005), 40 < 20(p < .005)$

allowed us to investigate a realistic range of task difficulties. The yaw and pitch distances are different since yaw has a lower angular range of wrist motion. Based on initial pilots, we mapped the wrist and forearm motion to pixels as follows: 1) For RotoWrist and GTW tracking, we translated a single degree of angular wrist motion along the yaw-pitch axis to 4.35 pixels along the x-y axis respectively. For GTF, a 1cm arm motion along the horizontal-vertical axis (rotating the forearm from the elbow) translated to 20 pixels along x-y respectively. In our pilot study, these numbers allowed all users to be able to reach the targets.

For each condition, participants performed 5 repetitions. We followed a within-subjects design where each participant performed all conditions. We counterbalanced Axis and Method among the participants using a Latin square and randomized the Distance and Width. We recruited 12 participants (25-50 years of old) for the study. All except one was right-handed. The study took 75 mins and participants were compensated for their time. In total, we had 12 participants \times 54 conditions \times 5 repetitions = 3240 trials.

6.2 Procedure

Participants sat on a chair in front of a computer display. To allow participants to use the keyboard on a hard surface, we placed a table in front of them as shown in Figure 8. We used the same data collection setup explained in Section 4 and calculated ground truth wrist orientations using Equation 4. The study software was written in PyGame.

Prior to beginning, participants were given a short instructional session in which they familiarized themselves with the tasks and how should they move their wrist or arm to move the cursor and select the target. The on-screen cursor appeared as a black dot and the targets appeared as red circles. We implemented a standard pointing task [1] where the next target with the appropriate distance and width appeared after the current selection. For selection, we used a keyboard and asked the users to hit the space-bar when they feel the black dot is in the red target. As is standard, we asked the users to perform the task as quickly and as accurately as possible. Participants were provided regular breaks.

6.3 Measures

We measure Movement Time (MT) – the time it took for the user to complete a trial, and Incorrect Trials (IT) – the number of incorrect trials out of five for each condition. An incorrect trial is when a user misses a target (i.e the space-bar is hit while the cursor is outside the target) or if the movement time is an outlier. We removed the incorrect trials from the movement time measurement.

6.4 Results

For each axis, we conducted 3-way repeated measures ANOVAs on movement time and incorrect trials. Greenhouse-Geisser corrections were applied for violations of sphericity. The results were similar for both axes. For both yaw and pitch, for Movement Time and Incorrect Trials, we found significant main effects of all three Method, Distance, and Width. No interaction effects were found. Table 1 shows the main effects statistics.

Pairwise comparisons with Bonferroni corrections (Table 1) showed that the effects of distance and width broadly adhered to Fitts' law with Movement Time increasing with increasing distance and decreasing with increasing width. Since there are no interaction effects, we focus on the effect of Method on Movement Time and Incorrect Trials.

6.4.1 Effect of Method. Figure 9 shows the movement time and incorrect trials for each method for both axes. Ground truth wrist is faster than ground truth forearm or RotoWrist according to the pairwise comparisons, although the difference is only 0.25s. This shows that users can complete the pointing task using RotoWrist across all distances and width while only being slightly slower than ground truth wrist tracking and similar to ground truth forearm tracking. A similar trend is observed in incorrect trials.

6.4.2 Adherence to Fitts' Law. Figure 10 illustrates the movement time as a function of index of difficulty (ID) for the three different methods among all participants. A linear regression model was used to fit the data. All three methods show adherence to Fitts' law, albeit a weak one given the lower R^2 values. This shows that alternate modeling approaches should be investigated to better model pointing based on hand-tracking.

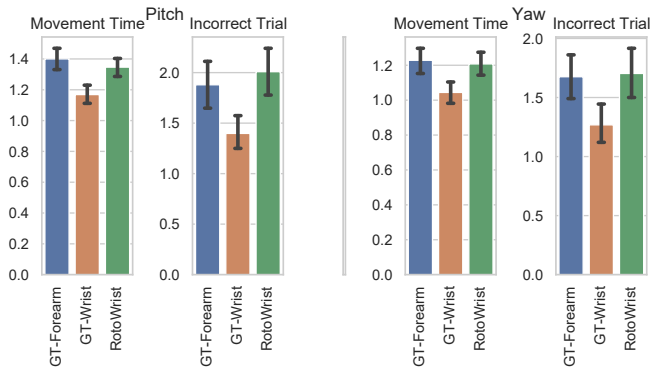


Figure 9: Mean and standard deviation of movement time and incorrect trials for pitch and yaw axis.

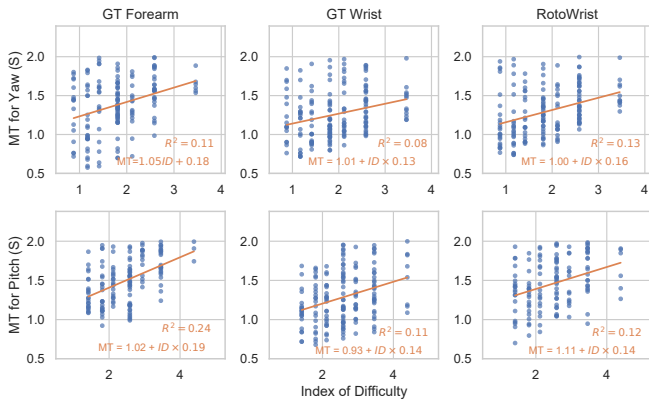


Figure 10: Yaw and Pitch Movement Time vs Fitts' ID

Overall, the results show that RotoWrist enables pointing tasks to be performed with performance that is only slightly below ground truth wrist tracking. Although the RotoWrist has similar performance in movement time and error rate to ground truth forearm tracking, it is still the preferred choice compared to ground truth forearm tracking since it requires less movement from the user and can be performed in a more subtle and comfortable manner. This was profoundly echoed by the participants feedback where they mentioned more fatigue when performing ground truth forearm movements for pointing task. Using a wearable device like RotoWrist to track wrist pose is also easier from an implementation perspective than enabling forearm tracking, which requires another point of instrumentation in the world or on the head (e.g., HMD-mounted cameras to track the arm).

7 APPLICATIONS

The ability to track one's wrist orientation reliably and precisely without user training enables a wide range of applications. We envision these applications to be with or without a HMD. In this section, we discuss and demonstrate two features that RotoWrist can enable.



Figure 11: A Rift-S controller is added to the controller armband to facilitate 6-DoF tracking of the hand.

7.1 Pointing

AR and VR platforms represent a promising direction for next-generation computing platforms. For many applications, being able to point at objects precisely is of a great importance. The handheld controller is a useful input device that is common in VR, but moving the hands without the encumbrance of holding a physical handheld controller could lead to more natural and casual experiences.

To demonstrate the potential of RotoWrist as a pointing device, we demonstrate how it can be used to play Beat Saber, one of the most popular VR experiences. The game is normally controlled by two handheld controllers, and is particularly challenging as it requires precise targeting and low-latency.

To build this demo, we attached a Rift-S handheld controller to the top of the controller armband as shown in Figure 11. The controller tracked the user's arm pose with respect to the headset. During a simple calibration phase, we determine the transformation from the pose of the Rift-S controller to the pose of the hand. At runtime, we add the wrist angles estimated from RotoWrist to the transformed pose of the controller to accurately capture the 6-DoF pose of the hand.

We asked ten users to try our demo for one song and provide feedback. We purposefully had them play the game using a Rift-S handheld controller on the right hand while having our device on their left hand so that they can compare the two input devices. Almost all users were very excited about the idea of playing BeatSaber without a handheld controller and were impressed by the tracking accuracy. Two people mentioned that they felt that RotoWrist was more delayed than the Rift-S handheld controller but not enough to make them uncomfortable. Further improvements in speed and accuracy may be possible by using a Kalman filter to proactively estimate the next wrist orientation.

7.2 Free-form Hand Drawing

To highlight RotoWrist's ability to perform fine-grained continuous tracking (beyond gestural swipes), we implemented a drawing application driven solely by the user's wrist orientation. Since the wrist has smaller range of motion in radial/ulnar deviation, the

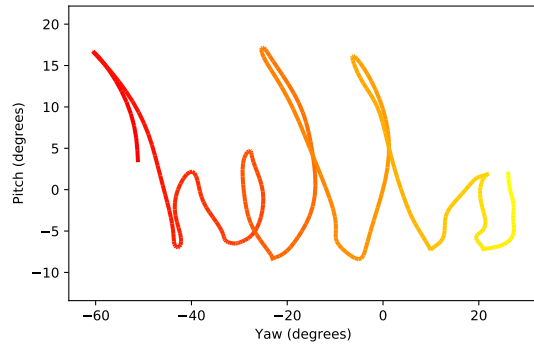


Figure 12: Handwriting examples using wrist-only motion.

drawing canvas shifts to the left by a few pixels each frame to enable an infinite canvas. This free-form drawing can be used to draw shapes for gestures recognition or can be used for handwriting reconstruction. Figure 12 shows a user that used RotoWrist to write "hello" in the mid air. With appropriate visual feedback, we anticipate the performance to be even better.

8 DISCUSSION

In this work, we demonstrated RotoWrist, a wearable wrist-worn device that enables precise tracking of the orientation of the wrist. Due to the simplicity of its tracking algorithm, RotoWrist does not require user training to work. We also showed that with minimal additional calibration, pitch and yaw accuracy improves and achieves an RMSE of 3.5° and 3.6° respectively.

8.1 Complementing Vision-based Wristband Tracking

We envision RotoWrist's use either with or without a head-mounted display. However, even though head-mounted cameras are getting better at tracking hands and fingers, they still require line-of-sight. In contrast, tracking a wristband with infrared fiducial markers is a much simpler task. The combination of RotoWrist with a wristband tracker that results in a complete 6-DoF tracking system, may be preferable over a handheld controller in some scenarios. For example, a user could comfortably interact with their hands at their side where computer vision might fail, then seamlessly move into the field-of-view of the cameras, which would begin tracking the arm or wristband pose, and start direct manipulations. As a standalone device, RotoWrist offers a rich input source for smartwatches. With RotoWrist, a user can provide input using their wrist while keeping their arm motionless at their side or resting on a table. With some modifications, we envision that RotoWrist can capture information about the pose of the fingers as well, e.g., detecting a fist vs a full extended hand for target selection. This could be useful in mid-air drag & drop interactions.

8.2 Limitations and Future Work

In this paper, we focused on how RotoWrist can be generalized across sessions and users. We will now discuss how RotoWrist

can be generalized across different palm posture, location on the forearm and rigidity. Although in our evaluations, we asked the participants to make a fist, we observed that the tracking holds even as the user opens their fist and starts moving their fingers. It's worth mentioning that the tracking error increases as the user moves their thumb or pinky finger outwards, making a motion that, to RotoWrist, appears similar to a radial/ulnar deviation motion. Future work should consider how additional modeling or the use of additional sensors can distinguish between finger motion and wrist motion.

Although RotoWrist achieves a cross-user RMSE of 5.9° and 6.8° for pitch and yaw, respectively, our system can be vulnerable to major changes in the location of the band. We expect this can be addressed by using a few seconds of online learning. Furthermore, a challenge in the design of any wristband is sizing it for an appropriate fit across users. We also wanted the wristband to be rigid in order for the ToF modules to be roughly at the same pose for all users. Incorporating these modules in a flexible band requires more attention as shifts in the position of the modules would degrade performance. Furthermore, the relative angle of each module with respect to the band is an important factor to consider. While incorporating RotoWrist in a flexible band, care should be taken so that the modules do not change orientation.

RotoWrist consists of the sensing wristband with eight ToF IR modules and a controller arm band that supplies power to the sensing wristband and handles data communicating back to a host PC. Here, we have focused on the design of the sensing wristband and optimizing the placement of the ToF IR modules. Incorporating the controller components into the wristband is a fairly straightforward task—most smart watches do have an MCU and Bluetooth. In designing the sensing wristband, we placed the ToF modules evenly around the wristband. RotoWrist's performance could be improved further by additional optimization of the number and placement of ToF modules on the wristband. Future work could also investigate tracking accuracy with fewer sensors.

If RotoWrist is combined with other tracking systems, e.g., an HMD-based hand tracker, the additional calibration step discussed in Sections 5.2 and 5.3 could be done automatically during the first few seconds of use. After this, the hand tracking from the headset can stop and RotoWrist will be used for tracking.

9 CONCLUSION

In this work, we demonstrated RotoWrist, a wearable wrist-worn device that performs continuous 2-degree-of-freedom (DoF) wrist tracking using ToF IR sensing modules. RotoWrist works across users without requiring user calibrations. The RotoWrist system consists of a wristband that uses eight ToF IR modules to continuously measure the absolute distance from the hand in real-time. As the user moves their wrist, the relative distance between the hand and each sensor changes and collectively RotoWrist uses these measurements to track 2-DoF wrist orientation—flexion/extension and radial/ulnar deviation. RotoWrist offers a rich input source for a variety of wearable devices, including smartwatches and HMDs.

ACKNOWLEDGMENTS

We wish to thank Slava Karulin, Richard Cardin, and Jeff Holter for their help in designing and building RotoWrist's hardware and physical prototype. We also like to thank Aria Fereydouni for his help in conducting the user studies.

REFERENCES

- [1] [n.d.]. ISO. 9421-9 Ergonomic requirements for office work with visual display terminals (VDTs) - Part 9: Requirements for non-keyboard input devices. International Organization for Standardization. 2000.
- [2] Javid Abbasov, Tom Horak, and Raimund Dachselt. 2018. Smartwatch-based Pointing Interaction. In *Mensch und Computer 2018 - Tagungsband*, Raimund Dachselt and Gerhard Weber (Eds.). Gesellschaft für Informatik e.V., Bonn. <https://doi.org/10.18420/muc2018-mci-0373>
- [3] Ke-Yu Chen, Kent Lyons, Sean White, and Shwetak Patel. 2013. UTrack: 3D Input Using Two Magnetic Sensors. In *Proceedings of the 26th Annual ACM Symposium on User Interface Software and Technology* (St. Andrews, Scotland, United Kingdom) (*UIST '13*). Association for Computing Machinery, New York, NY, USA, 237–244. <https://doi.org/10.1145/2501988.2502035>
- [4] Ke-Yu Chen, Shwetak N. Patel, and Sean Keller. 2016. Finexus: Tracking Precise Motions of Multiple Fingertips Using Magnetic Sensing. In *Proceedings of the 2016 CHI Conference on Human Factors in Computing Systems* (San Jose, California, USA) (*CHI '16*). Association for Computing Machinery, New York, NY, USA, 1504–1514. <https://doi.org/10.1145/2858036.2858125>
- [5] F. Cordella, F. Di Corato, G. Loianno, B. Siciliano, and L. Zollo. 2013. Robust pose estimation algorithm for wrist motion tracking. In *2013 IEEE/RSJ International Conference on Intelligent Robots and Systems*. 3746–3751. <https://doi.org/10.1109/IROS.2013.6696891>
- [6] Artem Dementyev and Joseph A. Paradiso. 2014. WristFlex: Low-power Gesture Input with Wrist-worn Pressure Sensors. In *Proceedings of the 27th Annual ACM Symposium on User Interface Software and Technology* (Honolulu, Hawaii, USA) (*UIST '14*). ACM, New York, NY, USA, 161–166. <https://doi.org/10.1145/2642918.2647396>
- [7] T. Deyle, S. Palinko, E. S. Poole, and T. Starner. 2007. Hambone: A Bio-Acoustic Gesture Interface. In *2007 11th IEEE International Symposium on Wearable Computers*. 3–10. <https://doi.org/10.1109/ISWC.2007.4373768>
- [8] Jun Gong, Zheer Xu, Qifan Guo, Teddy Seyed, Xiang “Anthony” Chen, Xiaojun Bi, and Xing-Dong Yang. 2018. WrisText: One-Handed Text Entry on Smartwatch Using Wrist Gestures. In *Proceedings of the 2018 CHI Conference on Human Factors in Computing Systems* (Montreal QC, Canada) (*CHI '18*). Association for Computing Machinery, New York, NY, USA, Article 181, 14 pages. <https://doi.org/10.1145/3173574.3173755>
- [9] Jun Gong, Xing-Dong Yang, and Pourang Irani. 2016. WristWhirl: One-handed Continuous Smartwatch Input Using Wrist Gestures. In *Proceedings of the 29th Annual Symposium on User Interface Software and Technology* (Tokyo, Japan) (*UIST '16*). ACM, New York, NY, USA, 861–872. <https://doi.org/10.1145/2984511.2984563>
- [10] Aakar Gupta, Cheng Ji, Hui-Shyong Yeo, Aaron Quigley, and Daniel Vogel. 2019. RotoSwype: Word-Gesture Typing Using a Ring. In *Proceedings of the 2019 CHI Conference on Human Factors in Computing Systems* (Glasgow, Scotland UK) (*CHI '19*). Association for Computing Machinery, New York, NY, USA, Article 14, 12 pages. <https://doi.org/10.1145/3290605.3300244>
- [11] Chris Harrison, Desney Tan, and Dan Morris. 2010. Skinput: Appropriating the Body as an Input Surface. In *Proceedings of the SIGCHI Conference on Human Factors in Computing Systems* (Atlanta, Georgia, USA) (*CHI '10*). Association for Computing Machinery, New York, NY, USA, 453–462. <https://doi.org/10.1145/1753326.1753394>
- [12] Fang Hu, Peng He, Songlin Xu, Yin Li, and Cheng Zhang. 2020. FingerTrak: Continuous 3D Hand Pose Tracking by Deep Learning Hand Silhouettes Captured by Miniature Thermal Cameras on Wrist. *Proc. ACM Interact. Mob. Wearable Ubiquitous Technol.* 4, 2, Article 71 (June 2020), 24 pages. <https://doi.org/10.1145/3397306>
- [13] Yasha Iravantchi, Mayank Goel, and Chris Harrison. 2019. BeamBand: Hand Gesture Sensing with Ultrasonic Beamforming. In *Proceedings of the 2019 CHI Conference on Human Factors in Computing Systems* (Glasgow, Scotland UK) (*CHI '19*). ACM, New York, NY, USA, Article 15, 10 pages. <https://doi.org/10.1145/3290605.3300245>
- [14] Yasha Iravantchi, Yang Zhang, Evi Bernitsas, Mayank Goel, and Chris Harrison. 2019. Interferi: Gesture Sensing Using On-Body Acoustic Interferometry. In *Proceedings of the 2019 CHI Conference on Human Factors in Computing Systems* (Glasgow, Scotland UK) (*CHI '19*). ACM, New York, NY, USA, Article 276, 13 pages. <https://doi.org/10.1145/3290605.3300506>
- [15] P. Jung, G. Lim, S. Kim, and K. Kong. 2015. A Wearable Gesture Recognition Device for Detecting Muscular Activities Based on Air-Pressure Sensors. *IEEE Transactions on Industrial Informatics* 11, 2 (April 2015), 485–494. <https://doi.org/10.1109/TII.2015.2405413>
- [16] Frederic Kerber, Pascal Lessel, and Antonio Krüger. 2015. Same-Side Hand Interactions with Arm-Placed Devices Using EMG. In *Proceedings of the 33rd Annual ACM Conference Extended Abstracts on Human Factors in Computing Systems* (Seoul, Republic of Korea) (*CHI EA '15*). Association for Computing Machinery, New York, NY, USA, 1367–1372. <https://doi.org/10.1145/2702613.2732895>
- [17] Wolf Kienzle and Ken Hinckley. 2014. LightRing: Always-Available 2D Input on Any Surface. In *Proceedings of the 27th Annual ACM Symposium on User Interface Software and Technology* (Honolulu, Hawaii, USA) (*UIST '14*). Association for Computing Machinery, New York, NY, USA, 157–160. <https://doi.org/10.1145/2642918.2647376>
- [18] David Kim, Otmar Hilliges, Shahram Izadi, Alex D. Butler, Jiawen Chen, Iason Oikonomidis, and Patrick Olivier. 2012. Digits: Freehand 3D Interactions Anywhere Using a Wrist-Worn Gloveless Sensor. In *Proceedings of the 25th Annual ACM Symposium on User Interface Software and Technology* (Cambridge, Massachusetts, USA) (*UIST '12*). Association for Computing Machinery, New York, NY, USA, 167–176. <https://doi.org/10.1145/2380116.2380139>
- [19] Gierad Laput, Robert Xiao, and Chris Harrison. 2016. ViBand: High-Fidelity Bio-Acoustic Sensing Using Commodity Smartwatch Accelerometers. In *Proceedings of the 29th Annual Symposium on User Interface Software and Technology* (Tokyo, Japan) (*UIST '16*). Association for Computing Machinery, New York, NY, USA, 321–333. <https://doi.org/10.1145/2984511.2984582>
- [20] Claus Falck Larsen, Finn K. Mathiesen, and Steen Lindequist. 1991. Measurements of carpal bone angles on lateral wrist radiographs. *The Journal of Hand Surgery* 16, 5 (1991), 888 – 893. [https://doi.org/10.1016/S0363-5023\(10\)80156-X](https://doi.org/10.1016/S0363-5023(10)80156-X)
- [21] Jaime Lien, Nicholas Gilliam, M. Emre Karagozler, Patrick Amihoud, Carsten Schwesig, Erik Olson, Hakim Raja, and Ivan Poupyrev. 2016. Soli: Ubiquitous Gesture Sensing with Millimeter Wave Radar. *ACM Trans. Graph.* 35, 4, Article 142 (July 2016), 19 pages. <https://doi.org/10.1145/2897824.2925953>
- [22] Jess McIntosh, Asier Marzo, and Mike Fraser. 2017. SensIR: Detecting Hand Gestures with a Wearable Bracelet using Infrared Transmission and Reflection. 593–597. <https://doi.org/10.1145/3126594.3126604>
- [23] Scott D. McPhee. 1987. Functional Hand Evaluations: A Review. *American Journal of Occupational Therapy* 41, 3 (03 1987), 158–163. <https://doi.org/10.5014/ajot.41.3.158> arXiv:[https://ajot.aota.org/aota/content_public/journal/ajot/930394/158.pdf](https://arxiv.org/abs/https://ajot.aota.org/aota/content_public/journal/ajot/930394/158.pdf)
- [24] Franziska Mueller, Florian Bernard, Aleksandr Sotnychenko, Dushyant Mehta, Srinath Sridhar, Dan Casas, and Christian Theobalt. 2018. GANerated Hands for Real-Time 3D Hand Tracking From Monocular RGB. In *The IEEE Conference on Computer Vision and Pattern Recognition (CVPR)*.
- [25] Rajalakshmi Nandakumar, Vikram Iyer, Desney Tan, and Shyamnath Gollakota. 2016. FingerIO: Using Active Sonar for Fine-Grained Finger Tracking. In *Proceedings of the 2016 CHI Conference on Human Factors in Computing Systems* (San Jose, California, USA) (*CHI '16*). Association for Computing Machinery, New York, NY, USA, 1515–1525. <https://doi.org/10.1145/2858036.2858580>
- [26] Farshid Salemi Parizi, Eric Whitmire, and Shwetak Patel. 2019. AuraRing: Precise Electromagnetic Finger Tracking. *Proc. ACM Interact. Mob. Wearable Ubiquitous Technol.* 3, 4, Article 150 (Dec. 2019), 28 pages. <https://doi.org/10.1145/3369831>
- [27] Siddharth S. Rautaray and Anupam Agrawal. 2015. Vision Based Hand Gesture Recognition for Human Computer Interaction: A Survey. *Artif. Intell. Rev.* 43, 1 (Jan. 2015), 1–54. <https://doi.org/10.1007/s10462-012-9356-9>
- [28] J. Rekimoto. 2001. GestureWrist and GesturePad: unobtrusive wearable interaction devices. In *Proceedings Fifth International Symposium on Wearable Computers*. 21–27. <https://doi.org/10.1109/ISWC.2001.962092>
- [29] Zhou Ren, Junsong Yuan, and Zhengyou Zhang. 2011. Robust Hand Gesture Recognition Based on Finger-Earth Mover's Distance with a Commodity Depth Camera. In *Proceedings of the 19th ACM International Conference on Multimedia* (Scottsdale, Arizona, USA) (*MM '11*). Association for Computing Machinery, New York, NY, USA, 1093–1096. <https://doi.org/10.1145/2072298.2071946>
- [30] Jaiyoung Ryu, William P. Cooney, Linda J. Askew, Kai-Nan An, and Edmund Y.S. Chao. 1991. Functional ranges of motion of the wrist joint. *The Journal of Hand Surgery* 16, 3 (1991), 409 – 419. [https://doi.org/10.1016/0363-5023\(91\)90006-W](https://doi.org/10.1016/0363-5023(91)90006-W)
- [31] T. Scott Saponas, Desney S. Tan, Dan Morris, Ravin Balakrishnan, Jim Turner, and James A. Landay. 2009. Enabling Always-Available Input with Muscle-Computer Interfaces. In *Proceedings of the 22nd Annual ACM Symposium on User Interface Software and Technology* (Victoria, BC, Canada) (*UIST '09*). Association for Computing Machinery, New York, NY, USA, 167–176. <https://doi.org/10.1145/1622176.1622208>
- [32] Arpita Ray Sarkar, G. Sanyal, and S. Majumder. 2013. Article: Hand Gesture Recognition Systems: A Survey. *International Journal of Computer Applications* 71, 15 (June 2013), 25–37. Full text available.
- [33] Shaishav Siddhpuria, Sylvain Malacria, Mathieu Nancel, and Edward Lank. 2018. Pointing at a Distance with Everyday Smart Devices. In *Proceedings of the 2018 CHI Conference on Human Factors in Computing Systems* (Montreal QC, Canada) (*CHI '18*). Association for Computing Machinery, New York, NY, USA, Article 173, 11 pages. <https://doi.org/10.1145/3173574.3173747>
- [34] Paul Strohmeier, Roel Vertegaal, and Audrey Girouard. 2012. With a Flick of the Wrist: Stretch Sensors as Lightweight Input for Mobile Devices. In *Proceedings of the Sixth International Conference on Tangible, Embedded and Embodied Interaction*

- (Kingston, Ontario, Canada) (*TEI '12*). Association for Computing Machinery, New York, NY, USA, 307–308. <https://doi.org/10.1145/2148131.2148195>
- [35] Jonathan Taylor, Lucas Bordeaux, Thomas Cashman, Bob Corish, Cem Keskin, Toby Sharp, Eduardo Soto, David Sweeney, Julien Valentin, Benjamin Luff, and et al. 2016. Efficient and Precise Interactive Hand Tracking through Joint, Continuous Optimization of Pose and Correspondences. *ACM Trans. Graph.* 35, 4, Article 143 (July 2016), 12 pages. <https://doi.org/10.1145/2897824.2925965>
- [36] Hoang Truong, Shuo Zhang, Ufuk Muncuk, Phuc Nguyen, Nam Bui, Anh Nguyen, Qin Lv, Kaushik Chowdhury, Thang Dinh, and Tam Vu. 2018. CapBand: Battery-free Successive Capacitance Sensing Wristband for Hand Gesture Recognition. In *Proceedings of the 16th ACM Conference on Embedded Networked Sensor Systems (Shenzhen, China) (SenSys '18)*. ACM, New York, NY, USA, 54–67. <https://doi.org/10.1145/3274783.3274854>
- [37] D. M. Vogt and R. J. Wood. 2014. Wrist angle measurements using soft sensors. In *SENSORS, 2014 IEEE*. 1631–1634. <https://doi.org/10.1109/ICSENS.2014.6985332>
- [38] L. Wang, K. Sun, H. Dai, W. Wang, K. Huang, A. Liu, X. Wang, and Q. Gu. 2019. WiTrace: Centimeter-Level Passive Gesture Tracking Using OFDM signals. *IEEE Transactions on Mobile Computing* (2019), 1–1.
- [39] Robert Wang, Sylvain Paris, and Jovan Popovič. 2011. 6D Hands: Markerless Hand-Tracking for Computer Aided Design. In *Proceedings of the 24th Annual ACM Symposium on User Interface Software and Technology (Santa Barbara, California, USA) (UIST '11)*. Association for Computing Machinery, New York, NY, USA, 549–558. <https://doi.org/10.1145/2047196.2047269>
- [40] Eric Whitmire, Farshid Salemi Parizi, and Shwetak Patel. 2019. Aura: Inside-out Electromagnetic Controller Tracking. In *Proceedings of the 17th Annual International Conference on Mobile Systems, Applications, and Services (Seoul, Republic of Korea) (MobiSys '19)*. ACM, New York, NY, USA, 300–312. <https://doi.org/10.1145/3307334.3326090>
- [41] Erwin Wu, Ye Yuan, Hui-Shyong Yeo, Aaron Quigley, Hideki Koike, and Kris M. Kitani. 2020. Back-Hand-Pose: 3D Hand Pose Estimation for a Wrist-Worn Camera via Dorsum Deformation Network. In *Proceedings of the 33rd Annual ACM Symposium on User Interface Software and Technology (Virtual Event, USA) (UIST '20)*. Association for Computing Machinery, New York, NY, USA, 1147–1160. <https://doi.org/10.1145/3379337.3415897>
- [42] Xing-Dong Yang, Tovi Grossman, Daniel Wigdor, and George Fitzmaurice. 2012. Magic Finger: Always-Available Input through Finger Instrumentation. In *Proceedings of the 25th Annual ACM Symposium on User Interface Software and Technology (Cambridge, Massachusetts, USA) (UIST '12)*. Association for Computing Machinery, New York, NY, USA, 147–156. <https://doi.org/10.1145/2380116.2380137>
- [43] Hui-Shyong Yeo, Juyoung Lee, Hyung-il Kim, Aakar Gupta, Andrea Bianchi, Daniel Vogel, Hideki Koike, Woontack Woo, and Aaron Quigley. 2019. WRIST: Watch-Ring Interaction and Sensing Technique for Wrist Gestures and Macro-Micro Pointing. In *Proceedings of the 21st International Conference on Human-Computer Interaction with Mobile Devices and Services (Taipei, Taiwan) (MobileHCI '19)*. Association for Computing Machinery, New York, NY, USA, Article 19, 15 pages. <https://doi.org/10.1145/3338286.3340130>
- [44] Hui-Shyong Yeo, Erwin Wu, Juyoung Lee, Aaron Quigley, and Hideki Koike. 2019. Opisthenar: Hand Poses and Finger Tapping Recognition by Observing Back of Hand Using Embedded Wrist Camera. In *Proceedings of the 32nd Annual ACM Symposium on User Interface Software and Technology (New Orleans, LA, USA) (UIST '19)*. Association for Computing Machinery, New York, NY, USA, 963–971. <https://doi.org/10.1145/3332165.3347867>
- [45] Yang Zhang and Chris Harrison. 2015. Tomo: Wearable, Low-Cost Electrical Impedance Tomography for Hand Gesture Recognition. In *Proceedings of the 28th Annual ACM Symposium on User Interface Software & Technology (Charlotte, NC, USA) (UIST '15)*. ACM, New York, NY, USA, 167–173. <https://doi.org/10.1145/2807442.2807480>